

## Phase Diagram of a Three-Orbital Model for High- $T_c$ Cuprate Superconductors

Cédric Weber,<sup>1,2</sup> T. Giamarchi,<sup>3</sup> and C. M. Varma<sup>4</sup>

<sup>1</sup>King's College London, Theory and Simulation of Condensed Matter (TSCM), The Strand, London WC2R 2LS, United Kingdom

<sup>2</sup>Thomas Young Centre, University College London, 17 Gordon Street, London WC1H 0AH, United Kingdom

<sup>3</sup>DPMC-MaNEP, University of Geneva, 24 Quai Ernest-Ansermet, CH-1211 Geneva, Switzerland

<sup>4</sup>Department of Physics and Astronomy, University of California, Riverside, California 92521, USA

(Received 29 May 2013; published 18 March 2014)

We study the phase diagram of an effective three-orbital model of the cuprates using variational Monte Carlo calculations on asymptotically large lattices and exact diagonalization on a 24-site cluster. States with ordered orbital current loops (LC), itinerant antiferromagnetism,  $d$ -wave superconductivity, and the Fermi liquid are investigated using appropriate Slater determinants refined by Jastrow functions for on-site and intersite correlations. We find an LC state stable in the thermodynamic limit for a range of parameters compatible with the Fermi surface of a typical hole doped superconductor provided the transfer integrals between the oxygen atoms have signs determined by the effects of indirect transfer through the Cu-4s orbitals as suggested by Andersen. The results of the calculations are that the LC phase gives way at lower dopings to an antiferromagnetism phase, and at larger dopings to superconductivity and Fermi liquid phases.

DOI: 10.1103/PhysRevLett.112.117001

PACS numbers: 74.72.-h, 71.27.+a, 74.20.-z, 78.35.+c

Intense effort has been devoted to the phase diagram of the high- $T_c$  superconductors [1], especially the pseudogap phase. Possibilities suggested for the latter include RVB and/or preformed superconducting pairs [2,3], loops of orbital current without broken translational symmetry (LC phases [4,5]) and with broken translational symmetry [6], and various other forms of lattice and magnetic order. The LC phases are worth investigating in detail because of neutron observations [7,8] in four different families of cuprates of moments well compatible with the existence of such phases. Their onset temperature is consistent with the pseudogap temperature  $T^*$  estimated from thermodynamic and transport measurements. The fluctuations of such phases [9,10] could provide a path to also explain the properties of the strange metal phase [11] as well as the  $d$ -wave superconductivity. However, several theoretical as well as experimental questions remain to be understood in relation to them.

In a quasi-1D system, it was found in weak-coupling renormalization group calculations and numerical approaches that longer-range interactions or a multiorbital nature of the unit cell are needed to stabilize the orbital current phases [12–14]. However, in one dimension these phases have a spatial modulation becoming incommensurate upon doping. Orbital current phases that do not break translational symmetry require a multiorbital model [15,16] that includes the orbitals of the copper as well as the oxygen in the unit cell. Three band Hubbard models were considered early in the literature [17], but the stability of orbital currents and loop current patterns was not investigated. In two dimensions, a mean-field analysis [4] of such a model showed the existence of the loop current phases when the

Cu-O nearest-neighbor repulsion is strong enough. However, although the mean-field result is independently confirmed [18], going beyond the mean field, either with exact diagonalizations [19,20] or by variational Monte Carlo (VMC) calculations [18] suggested an absence of currents for large lattice sizes for the canonical model of cuprates [15,21]. VMC calculations suggested, however, that the main ingredient for the existence of such current was the frustration in kinetic energy.

It is thus important to investigate more complete models in which alternative paths for the kinetic energy can provide such frustration. One such source of kinetic energy can be provided by apical oxygens [18]. Another possible source is additional kinetic energy terms [22] that have been suggested in addition to the direct transfer between the oxygen atoms. It was shown that the oxygen  $p_{x,y}$  orbital has a much larger overlap with the unoccupied copper 4s orbital than the direct O-O overlap, yielding on integration over the 4s orbital a different set of effective parameters, in which the effective O-O nearest-neighbor transfer integral can have a sign opposite to that of the direct transfer (for a derivation see the Supplemental Material [23]). We find and will explain that this strongly affects the stability of the loop current phase.

In this Letter we examine the role of such terms on the stability of orbital currents by performing a VMC investigation of the revisited three band Hubbard model of Ref. [22]. We use a Jastrow projected wave function that allows an unbiased investigation of the relative stability of a wide variety of phases including the loop current phase. The key issues that we address in this work are (i) what is the range of model Hamiltonian parameters which supports

the various phases, and (ii) is this range of parameter consistent with the Fermi surface of the typical hole doped cuprate and with the properties of the Mott insulator-AFM half-filled phase.

Our work builds on Ref. [18], only a short summary of the method is therefore given. The variational wave function considered here, and used as a variational ansatz for the three band model Hamiltonian of the cuprates [23], is built from the ground state  $\Psi_0$  of the Hofstadter-like Hamiltonian (in hole notations):

$$H^{MF} = \sum_{(i,j)} t_{ij} \chi_{ij} e^{i\theta_{ij}} c_{i\sigma}^\dagger c_{j\sigma} + \Delta \sum_{p\sigma} \hat{n}_{p\sigma} + \sum_i \mathbf{h}_i \cdot \mathbf{S}_i, \quad (1)$$

where  $\chi_{ij}$ ,  $\theta_{ij}$ , and  $\mathbf{h}_i$  are variational parameters. The variables  $\chi_{ij}$  and  $\theta_{ij}$  are allowed to be different on each bond for a unit cell.  $\theta_{ij} \neq 0$  is a requirement for time-reversal breaking through orbital currents; the geometry of flux within the unit cell is given by closed loops of  $\theta_{ij}$ . The local magnetic field  $\mathbf{h}_i$  allows antiferromagnetism with the Néel-type staggered structure. This procedure is used to determine the best approximation of the ground state of the fully interacting Hamiltonian for the cuprates (see Supplemental Material [23]).

Correlations and effects of quantum fluctuations of various kinds on the ground state wave functions (WFs) are included by multiplying  $\Psi_0$  by spin and charge Jastrow factors,  $\mathcal{J} = \exp(\sum_{i,j=1,N} v_{|i-j|}^c n_i n_j) \exp(\sum_{i,j=1,N} v_{|i-j|}^s S_i^x S_j^x)$ , where  $v_{|i-j|}^c$  and  $v_{|i-j|}^s$  are also variational parameters. We note that  $i = j$  in the charge Jastrow is equivalent to the local Gutzwiller projection. We considered Jastrow factors with  $|i - j| \leq 3$  Cu lattice spacings and checked that they are negligible beyond this. The minimization of the variational parameters is performed using a stochastic minimization procedure [24,25] in which the parameters of the uncorrelated part of the WF and the Jastrow parameters are minimized at the same time.

In the standard representation of the cuprates within a three band model, the curvature of the Fermi surface (for hole doped copper oxides) is given by the sign of  $t_{pp}$ . However, for the extended representation of Ref. [22], the two transfer integrals of the three band Hubbard model of the cuprates ( $t_{pp}$  and  $t_{pp}'$ ) control the curvature of the Fermi surface. This is very similar to one-band  $t - t' - U$  theories, where the curvature of the Fermi surface is controlled by the sign of the nearest- and next-nearest hopping  $t$  and  $t'$ . We emphasize, however, that the transfer integral  $t_{pp}'$  and  $t_{pp}$  do not have a direct equivalent in the single-band picture. The hopping  $t$ ,  $t'$ , and  $t''$  of the single band picture (see Ref. [26]) are obtained via nontrivial relations to the original parameters (transfer integrals of the original model and charge transfer energy).

The Fermi surface is in excellent agreement with the ARPES of LSCO for  $t_{pp}' = 1$  and  $t_{pp} = -0.3$  eV [see Fig. 1(b)]. These values are also consistent with their

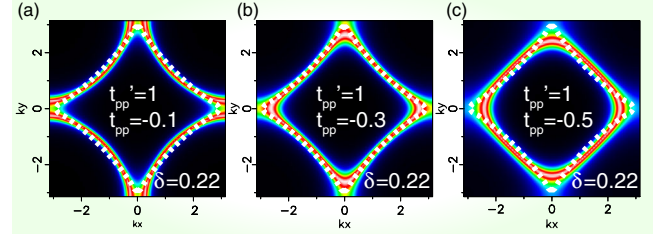


FIG. 1 (color online). Fermi surface of the uncorrelated Hamiltonian obtained for  $\Delta = 2$  eV and a)  $t_{pp} = -0.1$  eV, b)  $t_{pp} = -0.3$  eV, c)  $t_{pp} = -0.5$  eV for  $\delta = 22\%$  hole doping. The Fermi surface curvature is weakly dependent on the charge transfer energy  $\Delta$ , but evolves significantly with the oxygen-oxygen transfer integral  $t_{pp}$ . The Fermi surface of LSCO extracted from ARPES data is shown for comparison [28] (dotted lines).

derivation [23] and the magnitude of the direct O-O transfer of about 0.7 eV typically used. We also use  $t_{pp} = -0.5$  eV in the calculations in order to investigate the sensitivity of the results to this parameter. The transfer integrals  $t_{pp}$  and  $t_{pp}'$  are illustrated in Fig. 2(a). Controlled calculations [27] show that the charge transfer gap does not depend much on  $t_{pp}$  and  $t_{pp}'$ . Thus, observable properties in the insulating state are unaffected by the new choice.

We first discuss the low energy properties of a cluster of 8-CuO<sub>2</sub> cells (the Hamiltonian parameters are given in the Supplemental Material [23]) and compare the variational results to the exact ground state energy in Table I. As a reference, the energy of the Fermi-liquid (FL) state is shown. We first allow the WF which allows any time

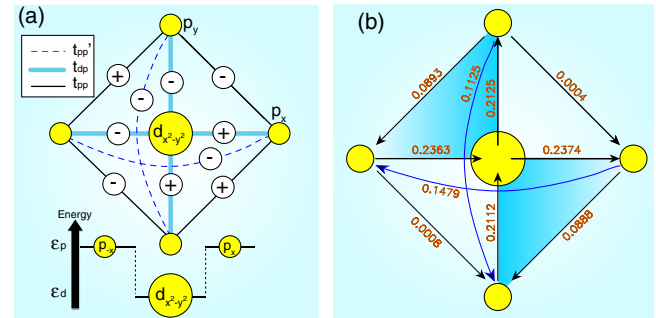


FIG. 2 (color online). (a) Signs of the charge transfer integrals in hole notations and definition of the model Hamiltonian parameters. The hopping  $t_{pp}$  (plain lines) connects the nearest neighbor O-p orbitals, the direct exchange  $t_{dp}$  (bold lines) connect the d and p orbitals, and  $t_{pp}'$  connects next nearest neighbor p orbitals (dashed lines),  $\epsilon_d$  ( $\epsilon_p$ ) are respectively the energy levels of the d and p orbitals. The signs of the transfer integrals are given on each link. (b) Pattern of current obtained from the variational w.f.  $\theta_2/J/LS$  on a 8-copper lattice with 10 holes and  $S^z = 0$  (see Table I). The current flows between orbitals lying on nearest neighbor sites (black arrow) and between along the  $p_x - p_x$  and  $p_y - p_y$  oxygens orbitals (blue arrows). The current pattern has two circulating current loops (shaded areas) with opposite chiralities.

TABLE I. Variational energies  $E$  and variance  $\sigma^2$  of the different WFs on an 8-cell  $\text{CuO}_2$  lattice with 10 holes ( $\delta = 25\%$ ) and  $S^z = 0$  together with the exact ground state energies ED for total momentum  $\mathbf{k} = (0, 0)$  and  $\mathbf{k} = (0, \pi), (\pi, 0)$ . The variational Ansatz are (i) the Fermi sea projected with a local Gutzwiller projection or Fermi-liquid (FL), (ii) the mean-field orbital current WFs in  $\theta_2$  pattern projected with a local Gutzwiller projection, (iii)  $\theta_2$  optimized with the Jastrow factors ( $\theta_2/J$ ), iv)  $\theta_2/J$  improved by applying additionally one Lanczos step ( $\theta_2/J/LS$ ). All shown results are for  $\Delta = 0$  and  $t_{pp} = -0.5$  eV. We also show the energy ( $E_{192}$ ) and variance ( $\sigma_{192}^2$ ) obtained on a 192 site lattice for comparison (with same  $\delta$ ). On the large lattice, both the energy and variance are systematically improved by the WF optimizations.

WFs	E [eV]	$\sigma^2$ [eV <sup>2</sup> ]	$J_{dp}$ [eV]	$E_{192}$ [eV]	$\sigma_{192}^2$ [eV <sup>2</sup> ]
FL	-1.700(1)	0.064(1)	0	-1.604(1)	0.0129(1)
$\theta_2$	-1.996(1)	0.0507(1)	0.29(1)	-1.657(1)	0.0102(1)
$\theta_2/J$	-2.023(1)	0.0409(2)	0.22(2)	-1.848(1)	0.0028(1)
$\theta_2/J/LS$	-2.077(1)	0.0498(1)	0.22(1)	-1.863(1)	0.0019(1)
ED ( $\mathbf{k} = (0, \pi)$ )	-2.1954(0)	0	0		
ED ( $\mathbf{k} = (0, 0)$ )	-2.1965(0)	0	0		

reversal symmetry breaking pattern (the complex phases are optimized on each of the link within a Cu-O<sub>2</sub> unit cell). Remarkably, we find that the orbital currents are stabilized and yield an effective energy optimization (see Table I, WF  $\theta_2$ ). The symmetry of the orbital current pattern (see Fig. 2) consists of two orbital current loops, with opposite chiralities, which is consistent with the theoretical proposal for the pseudogap phase of the cuprates [4].

The orbital current WF optimized with long-range Jastrow factors ( $\theta_2/J$ ) and with a so-called *Lanczos step* [29] ( $\theta_2/J/LS$ ) capture 95% of the ground state energy (ED). This suggests that the orbital current WF is a good candidate to describe the low energy physics of the three-band Hubbard model. Remarkably, we also find that the degenerate exact eigenstates in the  $\mathbf{k} = (0, \pi)$  and  $\mathbf{k} = (\pi, 0)$  are only 0.0009 eV ( $\approx 10$  K) apart from the ground state. The presence of very low energy states with finite momentum hint towards a possible orbital current instability [30].

Despite the good energy of our WFs, we notice that the obtained orbital current pattern for small lattices satisfies conservation of the current at each vertex to only within 10% or less (but with overall current 0), as shown in Fig. 2; this stems from the fact that the WF is not an eigenstate of the three band Hamiltonian, as discussed in Ref. [18].

In order to understand the physics of the orbital currents, we compare the change in the different contributions to the variational energies. As expected we find that the orbital current WF ( $\theta_2$ ), without any further optimization such as the Jastrow or the Lanczos step, reduces the double occupation, and reduces the local Coulomb energy from  $E_U = 0.42$  eV (FL) down to  $E_U = 0.31$  eV ( $\theta_2$ ), and also reduces the nearest-neighbor Coulomb repulsion from  $E_V = 0.54$  eV (FL) down to  $E_V = 0.22$  eV ( $\theta_2$ ). This large potential energy optimization due to orbital currents is accompanied by increased kinetic energy; in particular, the  $d$ - $p$  kinetic energy is worsened from  $E_{d-p} = -3.63$  down to  $E_{d-p} = -0.76$  eV, which is in turn largely compensated by a reduction of O-O kinetic energy from  $E_{p-p} = 0.97$

down to  $E_{p-p} = -1.77$  eV. Note that at low and moderate hole doping for  $t_{pp} < 0$ , the signs of the oxygen-oxygen overlaps in the Fermi liquid wave function are such as to give a positive contribution to the kinetic energy due to the  $t_{pp}$  term in the Hamiltonian. The orbital currents provide an efficient way to optimize both these and the interaction energy terms. This optimization is ineffective both at very low doping or for very large  $\Delta$ , where the  $t_{pp}$  kinetic term is negligible due to the low oxygen hole densities.

The importance of the sign of  $t_{pp}$  is that for chemical potential on the antibonding band of a three-orbital model, as in the cuprates, the orbital current phase is favored if the product of the signs of the transfer integrals around the O-Cu-O triangles is positive. This is already suggested by the fact that in such a triangle in isolation, the two degenerate current carrying (complex) states lie in energy above the one real state even for the noninteracting model.

Let us now consider the results for large clusters. We have performed calculations on lattices with 36, 64, and 100 unit cell sites, i.e.,  $N = 108$ ,  $N = 192$ , and  $N = 300$  lattice sites. In order to avoid spurious finite size effects induced by the artificial degeneracy of the variational wave functions, we considered rotated geometries, with  $T_1 = (L, 0)$  and  $T_2 = (1, L)$  lattice vectors, where  $L = 6, 8, 10$ , and we used periodic boundary conditions in all cases [31].

In Figs. 3(a) and 3(b), we show the condensation energy obtained for the orbital current  $\theta_2/J$  WFs, as a function of the charge transfer energy  $\Delta$  at fixed doping  $\delta \approx 12\%$  together with that for the  $d$ -wave superconducting phase. The superconducting wave function [see Figs. 3(a) and 3(b)] is obtained by replacing the Slater determinant with a  $d$ -wave BCS wave function and keeping the Jastrow factors. We find that the loop current instability is present at small and moderate charge transfer energy  $\Delta < 1$  eV. For large  $\Delta$  the three band Hamiltonian reduces to an effective one-orbital Hubbard or  $t$ - $J$  model, and no orbital currents are found. We find that at  $\delta = 12\%$  the  $d$ -wave BCS state is stabilized for  $\Delta > 1$  eV [Figs. 3(a) and 3(b)].

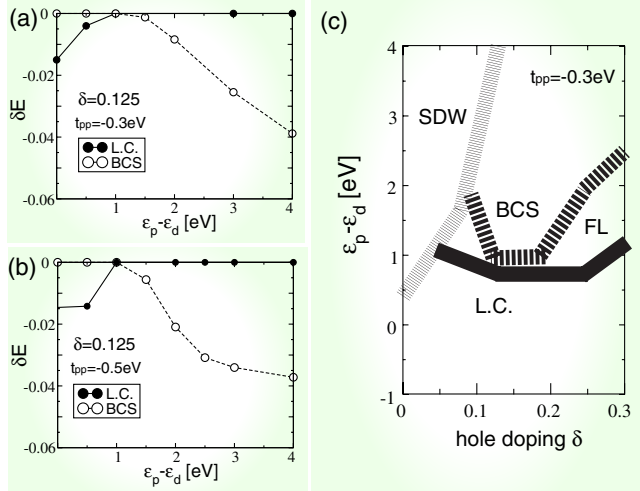


FIG. 3 (color online). Condensation energy  $\delta E$  of the loop current w.f. (filled circles) and of the d-wave superconducting wave-function (open circles) for 12.5% hole doping for a)  $t_{pp} = -0.3$  and b)  $t_{pp} = -0.5$ . Region of parameters where the different instabilities have the lowest energies for c)  $t_{pp} = -0.3$ . Labels refer to the Loop-current phase (LC), to the antiferromagnetic phase (SDW), to the superconducting d-wave instability (BCS), and to the Fermi liquid (FL). The width of the phase boundaries comes from both the statistical error bar in the calculations and from the discrete sampling of the phase space. Coexistence between the three different instabilities were not considered in this work. All calculations above are carried out for  $N = 192$ .

At zero doping we find that the Néel magnetic long-range order is stabilized for  $\Delta > 1$  eV, and is stable to increasing doping when the charge transfer energy is increased, in agreement with early variational Monte Carlo calculations done for the three band Hubbard model [32].

We summarize in Fig. 3(c) the phase diagram of the Fermi-liquid state and the states with the largest condensation energy for a given  $\Delta$  and  $\delta$ . The antiferromagnetic phase is obtained by removing the degeneracy of up and down spins in the Slater determinant corresponding to a commensurate  $(\pi, \pi)$  phase and with the Jastrow factors.

For  $t_{pp} = -0.3$  we recover the generic long-range ordered phases of the cuprates [Fig. 3(c)]. In particular, we obtain a stable AF state at low doping or large charge transfer energies (upper left part of the phase diagram). The loop current phase is obtained for moderate charge transfer energies and vanishes at larger charge transfer energies (stable in the lower part of the phase diagram). The superconducting instability is obtained at the vicinity of both the AF and LC states. We obtain, hence, a qualitative agreement with the phase diagram of the cuprates; however, whether the instabilities coexist and whether further improvements might shift the boundaries of the instabilities remain to be seen in future work. Further tweaking of the parameters in a small range (for example reducing  $t_{pp}$  by  $< 10\%$ ) about the chosen parameters is also likely to

reproduce the small variations of the ground states of the different cuprates compounds with doping.

We note that to compare with the cuprates, and to connect the charge transfer energy used in our calculations ( $\Delta = \epsilon_p - \epsilon_d$ ) with the physical charge transfer energy of the compounds ( $\Delta^0 = \epsilon_p^0 - \epsilon_d^0$ ), we need to correct the charge transfer energy with the double counting correction. Indeed,  $\Delta^0$  estimated from density functional theory already contains at the mean field level the effect of the correlation. The relation is  $\Delta = \Delta^0 - E_{DC}$ , and  $E_{DC} = U_d(n_d - 0.5)$ , where  $U_d$  is the Coulomb repulsion and  $n_d$  the hole density on Cu. With a typical value of  $n_d \approx 0.85$  [33], we obtain  $E_{DC} \approx 2.8$  eV. This is consistent with the observation of loop currents in LSCO for instance, where  $\Delta^0$  is estimated to be around 3–4 eV [34], which corresponds to  $\Delta \approx 0-1$  eV in our calculations.

Finally, we tested the validity of our results by extending the calculations to other values of the nearest neighbor Coulomb repulsion  $V_{dp}$  (see Supplemental Material [23]). We found that the orbital currents are stabilized for realistic values of the Coulomb repulsions  $V_{dp} < 3$  eV.

To summarize, we have carried out a detailed study of several broken symmetry phases of an effective three-orbital model for the cuprates, with the special new feature that it includes Cu-4s mediated oxygen-oxygen transfer, as suggested by Andersen [22]. This indirect O-O hybridization of Andersen leads to an ambiguity regarding the sign of the  $t_{pp}$  transfer integral. We have made a choice consistent with the direct  $t_{pp}$  and in agreement with the Fermi surface of a typical hole doped superconductor. We show that this new effective model for cuprates yields a stable LC phase at finite doping, consistent with the phase diagram suggested earlier and discovered by neutron scattering. We extended the calculations to large clusters by VMC calculations, and validate our theory by deducing a map of the amplitude of the orbital currents as a function of the doping and the charge transfer energy. The typical phases (spin density wave, loop current, superconducting and Fermi liquid) generically observed in the cuprates are also present in our calculations.

We thank Lijun Zhu, O.K Andersen, G. Kotliar, P. Bourges, and M. Greven for many illuminating discussions. This work was supported in part by the Swiss NSF under MaNEP and Division II. C.M.V. was supported by NSF Grant No. DMR-1206298. Part of the calculations were carried out on BlueGene/Q at the STFC Hartree Centre under Projects No. HCBG005 and No. HCBG073. We also gratefully acknowledge the support of NVIDIA Corporation with the donation of Tesla K20 GPUs used for this research.

- 
- [1] D. Bonn *Nat. Phys.* **2**, 159 (2006).
  - [2] G. Kotliar and J. Liu, *Phys. Rev. B* **38**, 5142(R) (1988).
  - [3] P. A. Lee, and X.-G. Wen, *Rev. Mod. Phys.* **78**, 17 (2006).

- [4] M. E. Simon and C. M. Varma, *Phys. Rev. Lett.* **89**, 247003 (2002).
- [5] C. M. Varma, *Phys. Rev. Lett.* **83**, 3538 (1999).
- [6] S. Chakravarty, R. B. Laughlin, D. K. Morr, and C. Nayak, *Phys. Rev. B* **63**, 094503 (2001).
- [7] B. Fauqué, Y. Sidis, V. Hinkov, S. Pailhès, C. T. Lin, X. Chaud, and P. Bourges, *Phys. Rev. Lett.* **96**, 197001 (2006).
- [8] Y. Li, V. Balédent, N. Barišić, Y. Cho, B. Fauqué, Y. Sidis, G. Yu, X. Zhao, P. Bourges, and M. Greven, *Nature (London)* **455**, 372 (2008).
- [9] V. Aji and C. M. Varma, *Phys. Rev. Lett.* **99**, 067003 (2007).
- [10] V. Aji, A. Shekhter, and C. M. Varma, *Phys. Rev. B* **81**, 064515 (2010).
- [11] C. M. Varma, P. B. Littlewood, S. Schmitt-Rink, E. Abrahams, and A. E. Ruckenstein, *Phys. Rev. Lett.* **63**, 1996 (1989).
- [12] E. Orignac and T. Giamarchi, *Phys. Rev. B* **56**, 7167 (1997).
- [13] U. Schollwock, S. Chakravarty, J. O. Fjaerestad, J. B. Marston, and M. Troyer, *Phys. Rev. Lett.* **90**, 186401 (2003).
- [14] P. Chudzinski, M. Gabay, and T. Giamarchi, *Phys. Rev. B* **78**, 075124 (2008).
- [15] C. M. Varma, S. Schmitt-Rink, and E. Abrahams, *Solid State Commun.* **62**, 681 (1987).
- [16] V. J. Emery, *Phys. Rev. Lett.* **58**, 2794 (1987).
- [17] R. T. Scalettar, D. J. Scalapino, R. L. Sugar, and S. R. White, *Phys. Rev. B* **44**, 770 (1991).
- [18] C. Weber, A. Lauchli, F. Mila, and T. Giamarchi, *Phys. Rev. Lett.* **102**, 17005 (2009).
- [19] M. Greiter and R. Thomale, *Phys. Rev. Lett.* **99**, 027005 (2007).
- [20] R. Thomale and M. Greiter, *Phys. Rev. B* **77**, 094511 (2008).
- [21] V. J. Emery, *Phys. Rev. Lett.* **58**, 2794 (1987).
- [22] O. K. Andersen, A. I. Liechtenstein, O. Jepsen, and F. Paulsen, *J. Phys. Chem. Solids* **56**, 1573 (1995).
- [23] See Supplemental Material at <http://link.aps.org/supplemental/10.1103/PhysRevLett.112.117001> for the methodology and additional data.
- [24] C. J. Umrigar, K. G. Wilson, and J. W. Wilkins, *Phys. Rev. Lett.* **60**, 1719 (1988).
- [25] S. Sorella, *Phys. Rev. B* **71**, 241103 (2005).
- [26] C. Weber, C. Yee, K. Haule, and G. Kotliar, *Europhys. Lett.* **100**, 37001 (2012).
- [27] X. Wang, L. deMedici, and A. J. Millis, *Phys. Rev. B* **83**, 094501 (2011).
- [28] A. Ino, C. Kim, M. Nakamura, T. Yoshida, T. Mizokawa, A. Fujimori, Z.-X. Shen, T. Kakeshita, H. Eisaki, and S. Uchida, *Phys. Rev. B* **65**, 094504 (2002).
- [29] The Lanczos step is carried out by minimizing the WFs in an extended parameter space ( $|\psi\rangle, \mathcal{H}|\psi\rangle$ ).
- [30] Note that the orbital currents cannot be directly observed in the Lanczos calculations, since the ground state of a finite system does not break spontaneously any symmetry, but remains in a superposition of quantum states.
- [31] For the specific case of the antiferromagnetic WFs we have considered bipartite lattices with  $T_1 = (L, 0)$  and  $T_2 = (0, L)$ ; see the text.
- [32] T. Yanagisawa, S. Koike, and K. Yamaji, *Phys. Rev. B* **64**, 184509 (2001).
- [33] C. Weber, K. Haule, and G. Kotliar, *Phys. Rev. B* **78**, 134519 (2008).
- [34] M. S. Hybertsen, M. Schluter, and N. E. Christensen, *Phys. Rev. B* **39**, 9028 (1989).